Thermal Design and Experimental Verification of the 3D-printed Registojet

Thermal Design and Experimental Verification of the 3D-Printed Resistojet

Daisuke Nakata[1]
Muroran Institute of Technology, Muroran,Hokkaido, 050-8585, Japan

and
Kiyoshi Kinefuchi[2]
Japan Aerospace Exploration Agency, Tsukuba, Ibaraki, 305-8505, Japan

A 3D-printed resistojet, wherein the heater and flow path were united, was produced. The heater consists of multi-layer shells and is difficult to break down. In this paper, the thermal design and the results of the thrust measurement are reported. The measured electrical resistance matched with the predicted one. Both the heater and the thrust reached 70 percent efficiency when paired with a nitrogen propellant at a mass flow rate of 0.2 g/s.

I. Nomenclature

c_p = specific heat
F = thrust
Isp = specific impulse
J = heater current
$\dot{m}$ = mass flow rate
P = input power
ΔT = temperature difference
η_p = heater efficiency
η_t = thrust efficiency

II. Introduction

Today, the use of all-electric satellites is attracting attention; generally, ion thrusters or Hall-effect thrusters are used for orbit-raising maneuvers with a specific impulse of 1000–3000 s[1]. The transfer time is usually 4–6 months, but a shorter trip time is attractive for commercial satellite use. A hydrogen-propelled resistojet is one of the competitive candidates. The specific impulse of the hydrogen-propelled resistojet is over 800 s at a chamber temperature of 2000 K[2]. The thrust-to-power ratio of the resistojet is inherently higher than that of ion/Hall thrusters, resulting in a shorter transfer time at a fixed power input.

The hydrogen-propelled electrothermal propulsion system has not been realized as a flight model because compact, long-term storage of hydrogen is impossible. Recent progress on thermal insulation technology allows for the consideration of a practical use of liquid hydrogen as a propellant for orbit-raising missions[3-4]. Of course, the term will be limited to a month.

III. Design and Theoretical Performance

In this study, the flow path of the propellant, which consists of multi-layer cylindrical shells, also functions as a single-piece heater for a resistojet. The propellant was fed from the outermost wall and heated as it enters the inner layer. This configuration prevents wasteful heat loss and realizes high-efficiency thermal insulation. Besides, the planar-shape heater is difficult to break as compared to a filament-type resistojet[5].

---

[1] Assistant Professor, Aerospace Plane Research Center, AIAA Member.
[2] Associate Senior Research Engineer, Research and Development Directorate, AIAA Senior Member.

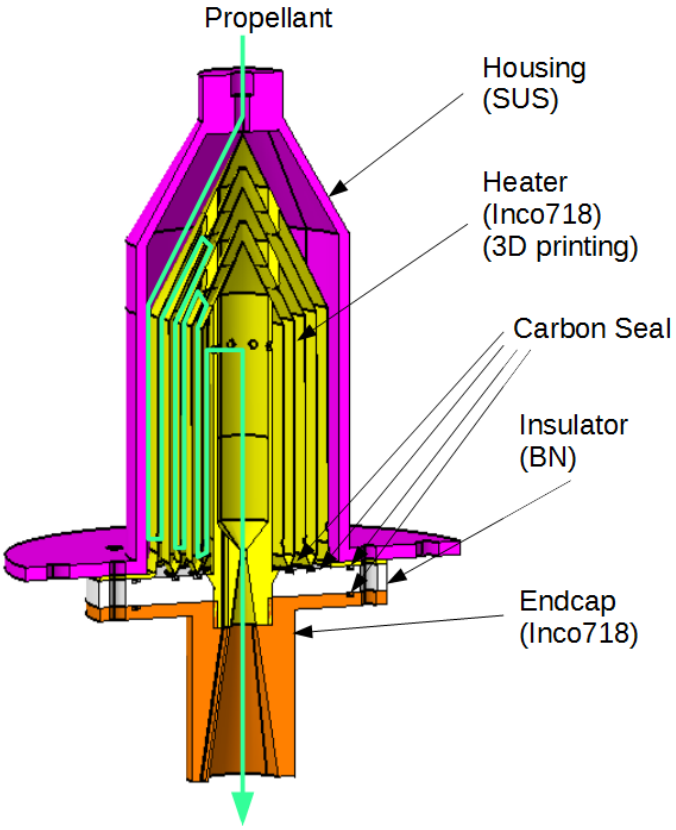

Fig. 1 3D-printed resistojet (3DRJ).

Figure 1 shows the cross-sectional view of the 3D-printed resistojet (3DRJ). The total weight is about 600g. The propellant passes along the light blue line as it is heated. Our overall objective is to make a single-piece tungsten heater, which can withstand 2000 K, but for now we have selected Inco 718 as the material of the conceptual model. The age-hardening heat treatment was not performed. EOS M-series printer was used for the manufacturing. As design guidelines of general additive manufacturing, the following parameters were taken into consideration:

1) A flat-topped ceiling should be avoided because a 3D printer laminates the structure from the bottom.
2) The wall thickness was set to 0.2 mm.
3) Laminating height has a maximum of 12 cm given a wall thickness of 0.2 mm.

The metal 3D printing used in this study works as follows:

1) A thin layer of metal powder is spread over the platform.
2) Then, high power laser scans the cross section of the component, melting the metal particles.
3) This process is repeated until the whole part is complete.
4) When the build process is finished, the parts are fully immersed in the metal powder.
5) Finally, the excess powder is removed manually or by vacuum cleaner.

In step five, the nozzle throat diameter was set to 2mm—insufficient powder removal results in a short circuit between layers. The other components in Fig.1 begin with housing, placed outside of the heater, made of stainless steel. Additionally, the propellant port is located at the top of the housing, and the electrical connection (GND) is on the flange face of the housing. Also, the end cap, made of Inconel 718, is located downstream of the heater nozzle. The other side of the electrical connection (V+) is attached to the flange face of the end cap, and the insulator, made of boron nitride, is sandwiched between the housing and the end cap. Finally, carbon seals are used to prevent gas leaks.

A. Electrical Resistance

In order to have a higher electrical resistance, a smaller gap between the heater walls and a large number of the layers is desirable. Design A7 had a six-layer heater, which consisted of layer 0(innermost), 1d, 1u, 2d, 2u and 3d, as shown in Fig. 2. The thickness of layer 0 was 1 mm in order to avoid the thermal distortion of the plenum chamber and the throat, whereas the thickness of the other layers is 0.2 mm. The gaps between the layers were set to 3 mm because of a concern about unexpected short circuiting due to thermal expansion. Table 1 shows the estimated electrical resistance of each layer and the estimated heater power at 100 A of current. The resistance in the outer layers is small, so the increase in the total heater power will be limited even if the number of layers is increased.

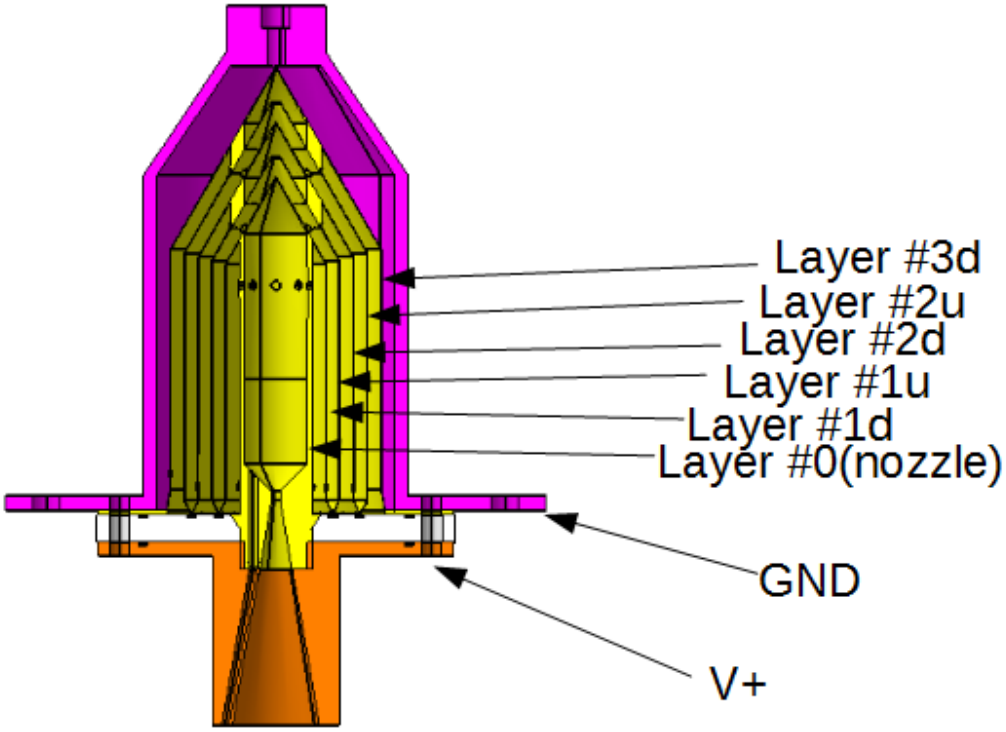

Fig. 2 The names of each layer.

Table 1 The relationship between the resistance in each layer and the theoretical heater power.

Layer Number	Mean radius, mm	Resistance, mΩ	Heater power, W
0 (nozzle)	6.5	1.8	19
1d + 1u	12.5	9.6	96
2d + 2u	18.5	6.5	65
3d	23	2.6	26
Total		20.5	206

*at a current of 100 A

B. Thermal Design

The heater walls heat the propellant while the propellant cools the heater walls. The maximum allowable temperature of the heater wall is considered to be about 900 K; the yield stress sharply decreases at this approximate temperature. The flow rate and the current should be controlled so that the hottest part of the heater—the plenum chamber wall—does not exceed the maximum allowable temperature. The propellant flow is choked at the throat, and pressure loss anywhere outside the throat is negligible. Table 2 shows the mass flow rate at 0.3 MPa of plenum pressure. A larger plenum temperature results in a lower mass flow rate because of the lower gas density.

Table 2 Choked mass flow rate at 2-mm diam. throat.

Gas	Plenum temperature, K	Mass flow rate, g/s
H_2	300	0.58
H_2	900	0.33
N_2	300	2.16
N_2	900	1.25

*at a plenum pressure of 0.3 MPaA

Quasi one-dimensional analyses were conducted in order to estimate the temperature rise throughout the flow path. Figure 3 illustrates the schematic image of the heat transfer between the propellant gas nodes (blue: Tg1-42) and the solid wall nodes (yellow: Tw7-42). Except for the outermost and innermost layers, one blue node exchanges heat with two yellow nodes.

The model assumes cylindrical coordinates, and the unit area per node is smaller on the inside. After establishing the initial propellant temperature, the mass flow rate, the heat-transfer coefficient and input current, the temperatures at each node are uniquely determined by solving a matrix,

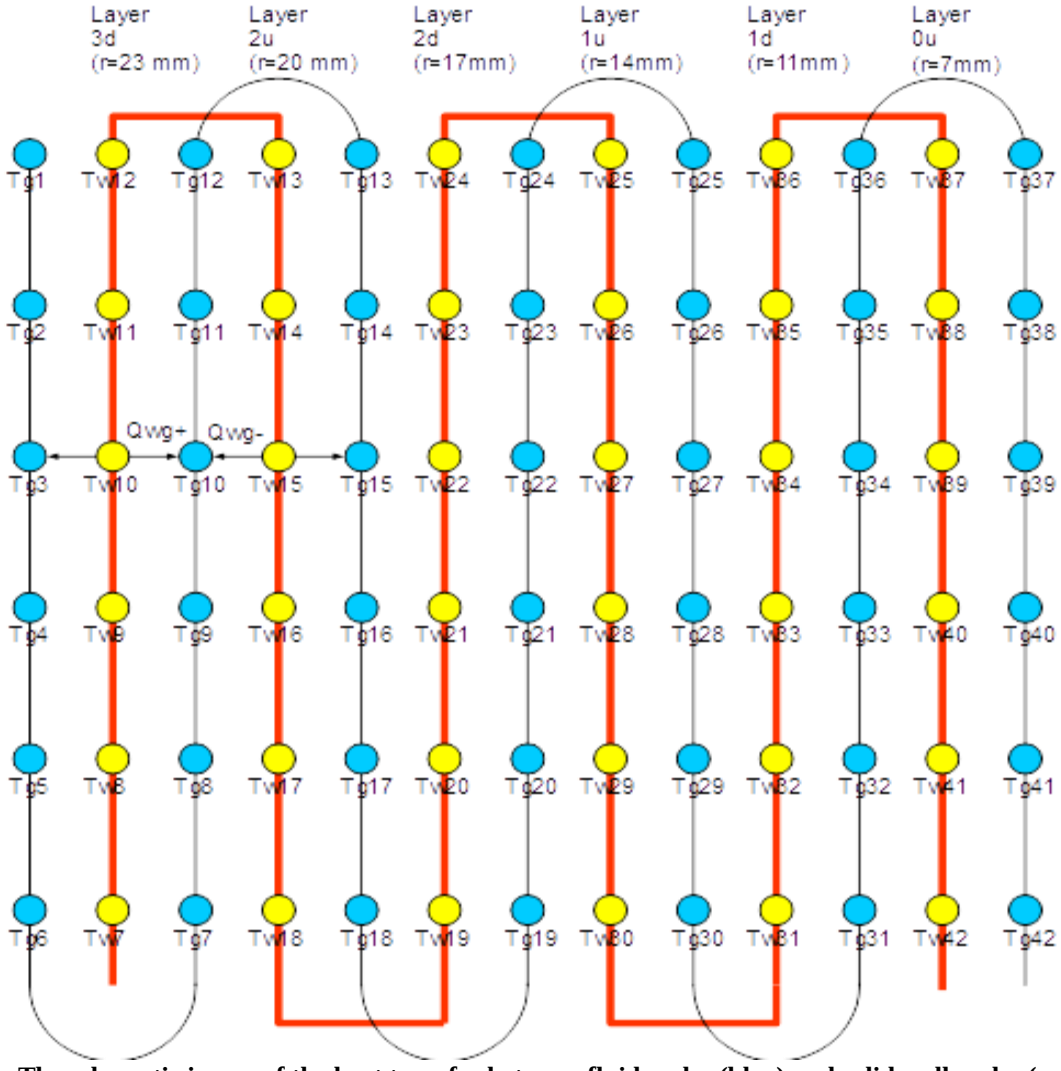

Fig. 3 The schematic image of the heat transfer between fluid nodes (blue) and solid wall nodes (yellow).

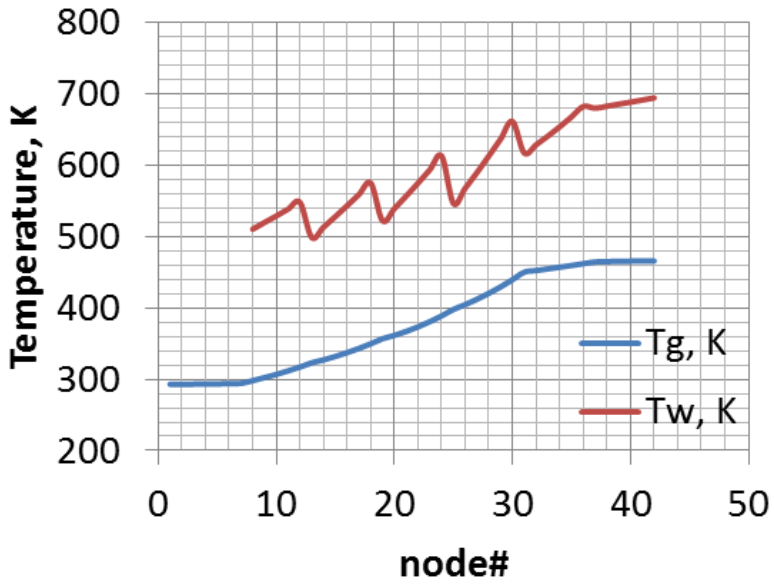

Fig. 4 Calculated temperature distribution. (N_2 propellant, $\dot{m}$=1 g/s, J = 100 A and h=43 W/m^2-K).

Figure 4 displays a temperature distribution along the node number. In this case, 1 g/s of the mass flow rate, 100 A of the current, and 43 W/m^2-K of the heat-transfer coefficient between the propellant and the walls were given as conditions. A heat transfer coefficient was determined based on the laminar flow on the plate, assuming Re = 3000. The maximum wall temperature reaches 693 K, but the exit-gas temperature is only 460 K. There is a big temperature gap between these temperatures because the heat transfer coefficient of nitrogen is small. A zig-zag shape on the wall temperature appears every six nodes—the temperature become small at nodes after the wall layers.

Table 3 shows the upper limit current in which the maximum wall temperature reaches 900 K, changing the mass flow rate. Table 4 shows the maximum wall temperature at fixed current, changing the heat transfer coefficient.

Table 3 Upper limit current at various mass flow rate conditions.

Mass flow rate, g/s	0.1	0.2	0.5	1.0
Current, A	52	73	103	123
Heat transfer coefficient, W/m^2-K	43	43	43	43
Exit gas temperature, K	851	785	664	554
Maximum wall temperature, K	900	900	900	900

Table 4 Maximum wall temperature at various heat transfer coefficients.

Mass flow rate, g/s	1.0	1.0	1.0	1.0
Current, A	100	100	100	100
Heat transfer coefficient, W/m^2-K	20	40	80	160
Exit gas temperature, K	464	465	468	472
Maximum wall temperature, K	962	713	590	532

Tables 3 and 4 explain basic principles of this resistojet. Table 3 shows that the enthalpy given to the propellant is constant at a fixed current, and the *Isp* simply increases by reducing the mass flow rate. (Here we assume 100 % heater efficiency; thus, no heat loss exists.)

As for Table 4, the smaller heat transfer coefficient results in a larger temperature difference between the gas and wall temperatures; therefore, a larger heat transfer coefficient is desirable for a higher gas temperature. In the next section, the experimental result of 3DRJ-A7 is compared to such theoretical principles.

IV. Experimental Results

A. Printed Heater Resistance

Figure 5 is a half-cut model of the manufactured 3DRJ. The roughness of the surface was of the order of 10 μm.

Fig. 5 Half-cut model of the manufactured 3D-RJ (design A7).

The measured total resistance of the heater (accomplished via the 4-terminal method) was 21.4 mΩ—5 % higher than expected (Table 1). This is caused by inaccurate printing thickness, but it is within a tolerable level. Note that the resistance determined from the voltage and current at the thrust measurement was 25.5 mΩ. This includes the contact resistance at the connection point.

B. Thrust Measurement

The thrust was measured in a vacuum chamber using nitrogen gas as a propellant. The results are shown in Table 5. The mass flow rate was determined using the upstream pressure, assuming limited flow at the throat. The nozzle temperature was measured by a thermocouple inserted through the nozzle exit. Each test case was performed twice: once for the nozzle exit temperature measurement and once for the thrust measurement, removing the thermocouple. Heater efficiency was determined by Eq. 1, and the thrust efficiency was determined by Eq. 2.

Table 5 Test results (Nitrogen gas).

Test Number	1	2	3	4
Mass flow rate, mg/s	47	108	102	221
Current, A	51	51	75	75
Input power, W	66	66	145	145
Thrust, mN	42	101	112	234
Specific Impulse, s	91	96	112	108
Nozzle Temperature, K	671	616	846	747
Specific Power, kJ/g	1.4	0.61	1.4	0.65
Heater Efficiency, %	28	55	40	72
Thrust Efficiency, %	29	72	42	85

$$\eta_p = \frac{\dot{m} c_p \Delta T}{P} \tag{1}$$

$$\eta_t = \frac{F^2}{2\dot{m}P} \tag{2}$$

The relationship between the mass flow rate and the thrust is shown in Figure 6. The thrust at $J = 0$ A indicates a cold flow thrust. At $J = 50$ A, 70 A, the thrust was slightly increased. Figure 7 shows the relationship between the input power and the specific impulse. The specific impulse was 85 s at $J = 0$ A and increased with the input power. Figures 8 and 9 show the heater efficiency and the thrust efficiency. Both the heater efficiency and the thrust efficiency increased with the mass flow rate. This is because the heat transfer coefficient became larger at larger densities and flow speeds.

As previously mentioned, the pure resistance of the heater was 21.4 mΩ and the total resistance, including the connection point, was 25.5 mΩ This implies that the possible upper limit in heater efficiency is 83 % based on Eq. 1, and 17 % of the input power is always a heat loss at the contact point. Therefore, 72 % of heater efficiency at test number 4 is not so bad. At any rate, it is necessary to design the heater resistance to be large enough that the contact resistance can be ignored.

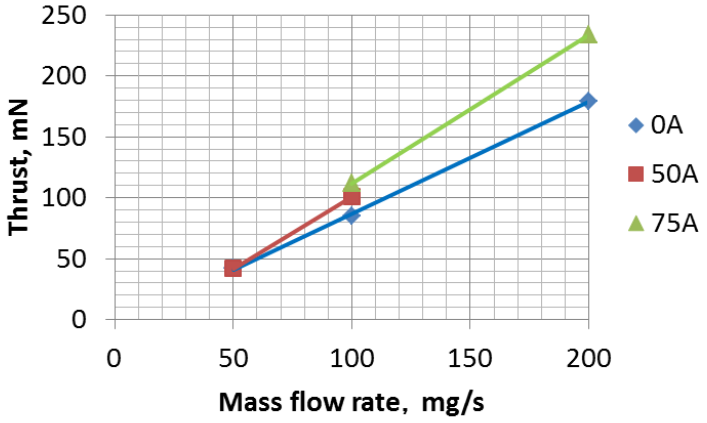

Fig. 6 The relationship between mass flow rate and thrust.

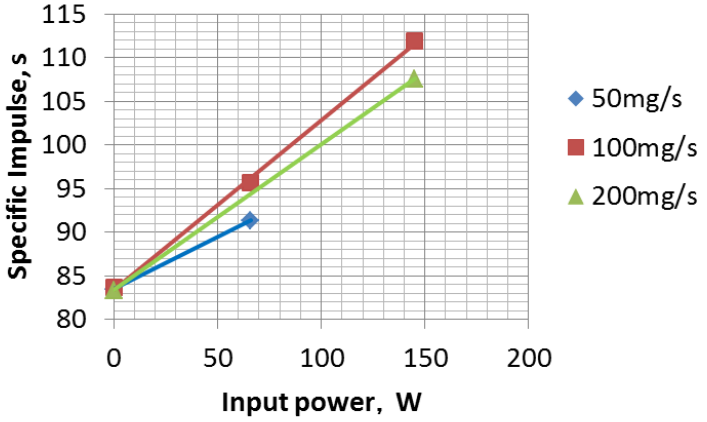

Fig. 7 The relationship between input power and specific impulse.

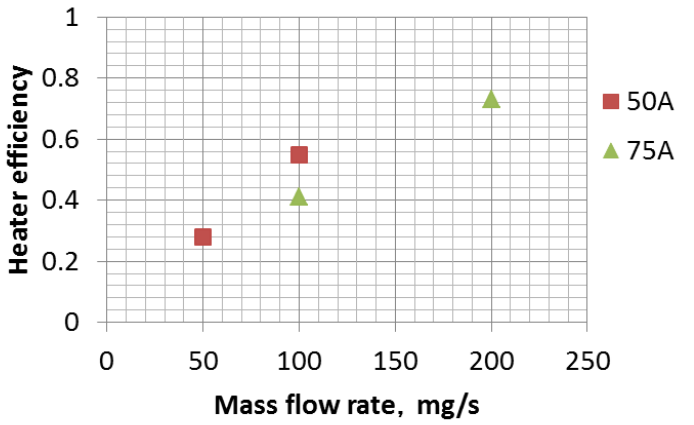

Fig. 8 The relationship between mass flow rate and heater efficiency.

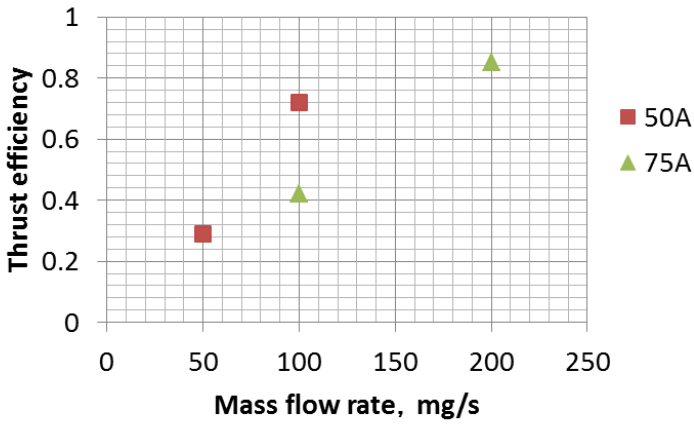

Fig. 9 The relationship between mass flow rate and thrust efficiency.

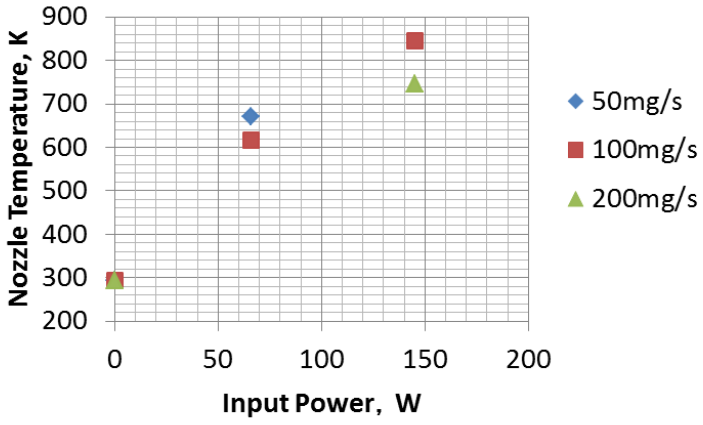

Fig. 10 The relationship between input power and nozzle temperature.

Table 6 The comparison between the preliminary analysis and the experimental results

Test Number	1	2	3	4
Mass flow rate, g/s	0.05	0.1	0.1	0.2
Current, A	50	50	75	75
Heat transfer coefficient, W/m^2-K	43	43	43	43
Estimated exit gas temperature, K	1161	807	1450	806
Measured exit gas temperature, K	671	616	846	747

Figure 10 shows the experimentally measured exit gas temperatures. In Table 6, experimental and preliminary estimated gas temperatures based on the quasi-one-dimensional calculation described in the previous section were compared. In the cases of 1 and 3, where the specific power was large and the heater efficiency was low, there was a large difference between the estimated and the experimental temperature. In the case of 4, where the heater efficiency was high, the estimated exit gas temperature was close to the experimented value.

All the estimates in Tables 3 and 4 were based on a heater efficiency of 100%, but this is the ideal assumption. Actually, a lower mass flow rate results in lower heater efficiency.

V. Design Improvement for Practical Use

A. Design Guidelines

It is important to enhance heat transfer in fixed operating conditions. Some design guidelines are suggested as follows:

1) Reduce the gap between layers and increase the number of layers.
2) Reduce the local thickness of the wall while maintaining the structural strength. This requires an adaption of the isogrid structure.
3) Increase the surface roughness to enhance the turbulent flow transition at lower flow rates.

Figures 11 and 12 show the design A11, reflecting all of the above guidelines. A11 realized 1.5 mm of the gap between the layers and the number of layers was increased to 14 at the same heater diameter. The thermal expansion was estimated to be 0.4 mm at 900 K, and we considered the risk of the short circuit to be small. Originally, the possible thickness was 0.2 mm due to the structural limitation. However, the increment of the heater resistance was realized by adopting an isogrid texture on the heater surface. The predicted electrical resistance was 80mΩ, which is four times larger than that of A7 design. Besides, now we are trying to make a tungsten resistojet with tungsten as a heater material.

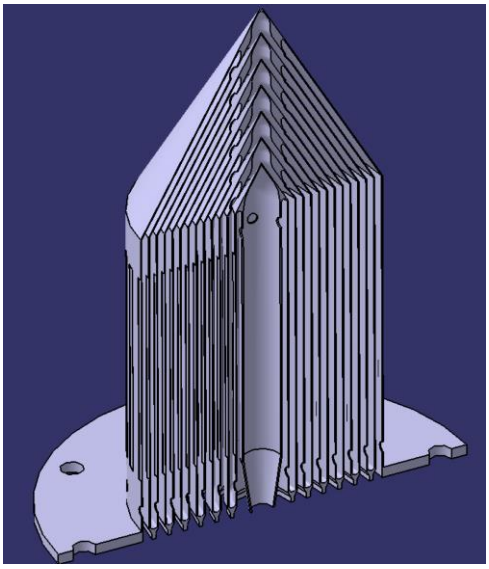

Fig. 11 The heater flow path of the 3DRJ-A11.

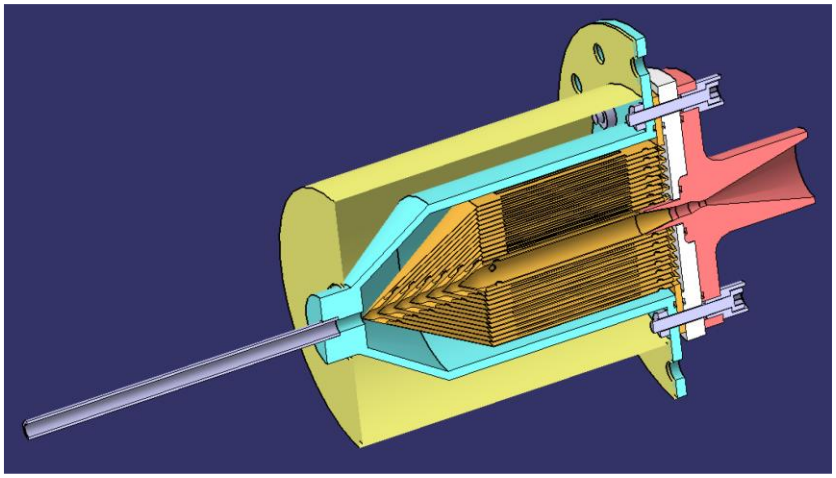

Fig. 12 Whole structure of the 3DRJ-A11.

B. Performance Prediction of the Tungsten Heater with a Hydrogen Propellant.

As mentioned in the introduction, we ultimately decided on the use of a tungsten heater and hydrogen gas in order to make this concept competitive. Table 7 shows a performance prediction of the tungsten resistojet with the hydrogen propellant, assuming an A7 design and 100 % of the heater efficiency. Here we set the maximum wall temperature to be 2000 K where the reduction of the yield stress is significant. The current model was directed not to exceed this maximum temperature restriction. Since the heat transfer coefficient of hydrogen is very high, the difference between the gas and the wall temperature is generally small as compared with nitrogen.

Table 7 Performance prediction of a tungsten-made 3DRJ with hydrogen propellant.

Mass flow rate, g/s	0.02	0.05	0.1
Current, A	159	217	320
Input power, W	544	1012	1854
Heat transfer coefficient, W/m^2-K	333	333	333
Exit gas temperature, K	1980	1904	1697
Maximum wall temperature, K	2002	1998	1978
Specific Impulse, s	752	650	460

*Assuming 100 % of heater efficiency

The performance at the mass flow rate of 0.02 g/s looks very promising, but actually the heater efficiency will be low in such a low mass flow rate. On the other hand, the heater efficiency will be high at 0.1 g/s of mass flow rate, but the performance is not so attractive.

VI. Conclusion

A 3D-printed resistojet, in which the heater and the flow path are united, was manufactured and tested.

- A 3D printer successfully molded a 0.2-mm-thick flow path. The measured resistance corresponded well to the preliminary estimation.
- A thrust measurement in a vacuum chamber with nitrogen gas was conducted. A heater efficiency of 70 % was achieved at a mass flow rate of 0.1 g/s. The measured nozzle exit temperature was close to the estimated value when the heater efficiency was high.
- In order to achieve the higher heater efficiency, the heat transfer coefficient between the gas and the walls should be increased. Reduction of the gap between layers, reduction of the wall thickness and adequate surface roughness increases this efficiency.
- Based on the manufactured design, a performance prediction of tungsten resistojet with hydrogen propellant was conducted. The specific impulse of 752 s is achieved at 2000 K of the maximum heater temperature.

References

[1] Caleb Henry., "All-electric satellites halfway to becoming half of all satellites," *Space News*, URL: http://spacenews.com/all-electric-satellites-halfway-to-becoming-half-of-all-satellites/ [retrieved 22 Aug. 2017].

[2] Russell, J., P., Carl, R., H. and Robert, A., S. "3-kw Concentric Tubular Resistojet Performance," Journal of Spacecraft, Vol. 3, No.11, pp. 1669-1674, 1966. doi: 10.2514/3.28723

[3] Mike Meyer, "Cryogenic Propellant Storage & Transfer (CPST) Technology Demonstration Mission (TDM)," URL: https://www.nasa.gov/pdf/743213main_CPST_Tech_Maturation.pdf [retrieved 1 Jun. 2018].

[4] Kiyoshi Kinefuchi, Koichi Okita, Hitoshi Kuninaka, Daisuke Nakata, and Hirokazu Tahara, "Preliminary Study of High Power Hydrogen Electric Propulsion for the Space Exploration", 50th AIAA/ASME/SAE/ASEE Joint Propulsion Conference, AIAA Propulsion and Energy Forum, AIAA 2014-3507, 2014. doi:10.2514/6.2014-3507

[5] Morren, W., E., "Performance and Endurance Tests of a Multipropellant Resistojet for Space Station Auxiliary Propulsion," NASA TM 87278, 1986.